Citation
Jin, H. and Hao, H. and Chen, W. and Xu, C. 2021. Spall Behaviors of Metaconcrete: 3D Meso-Scale Modelling. International Journal of Structural Stability and Dynamics. 21 (9): ARTN 2150121. http://doi.org/10.1142/S0219455421501212

Spall behaviors of metaconcrete: 3D meso-scale modelling

Hexin Jin [a,b], Hong Hao [b*], Wensu Chen [b*], Cheng Xu [b]

[a] School of Civil Engineering, Tianjin University, Tianjin 300350, China

[b] Centre for Infrastructural Monitoring and Protection, School of Civil and Mechanical Engineering, Curtin University, Australia

[*]Corresponding authors: hong.hao@curtin.edu.au (H. Hao), wensu.chen@curtin.edu.au (W. Chen)

Abstract

Spalling is a typical tensile fracture phenomenon due to insufficient tensile strength of concrete. Concrete structure might experience severe spall damage at the rear surface of the structure owing to reflected tensile stress wave induced by impulsive load. In recent years, metaconcrete consisting of engineered aggregates has attracted attentions as metaconcrete exhibits extraordinary wave-filtering characteristics. Metaconcrete can be used to attenuate stress wave generated by impulsive load and hence possibly mitigate the spall damage. In this study, engineered aggregate is designed via the software COMSOL to have the frequency bandgap coincide with the dominant frequency band of stress wave propagating in the normal concrete (NC) specimen to reduce the stress wave propagation and hence spall damage. The wave propagation behaviors in metaconcrete specimen with periodically distributed engineered aggregates have been investigated in a previous study. This study establishes 3D meso-scale model of metaconcrete including mortar, randomly distributed natural aggregates and engineered aggregates to simulate spall behaviors of metaconcrete via the software LS-DYNA. The responses of metaconcrete composed of engineered aggregates with single bandgap and multiple bandgaps are studied. The results show that stress wave can be more effectively attenuated by using engineered aggregates with multiple bandgaps. It is found that although engineered aggregates mitigate stress wave propagation, the soft coating of the engineered aggregates reduces the concrete material strength, therefore spall damage of metaconcrete specimen is not necessarily less severe than the normal concrete, but has different damage mode. In addition, the influences of loading intensity and duration on stress wave, as well as the spall behaviors of

metaconcrete specimen are also studied.

Keywords: Metaconcrete; Spall test; Meso-scale model; Impulsive load

1. Introduction

Concrete is the most widely used construction material [1, 2]. When impulsive load with the characteristics of short duration and high intensity is applied on a concrete structure, compressive stress wave is generated in the structure. When the compressive stress wave reaches the rear surface of the structure, it reflects at the free surface and turns into a tensile stress wave. The incident and reflected stress waves superpose at the rear of the concrete structure. If the net primary stress caused by the superposition of the stress waves exceeds the tensile strength of concrete, the concrete structure may experience spall damage with flying fragments [3, 4]. The flying fragments caused by the spall damage pose great threat to the surrounding personnel and equipment. Therefore, it is essential to study the dynamic tensile properties of concrete under high strain rate loads [5].

Experimental methods to measure dynamic tensile properties of concrete include spall test [6, 7], direct tensile test [8, 9] and Brazilian splitting test [10]. For the direct tensile test and the Brazilian splitting test, the strain rate of concrete can reach up to about 20 s^{-1}. However, concrete material may experience the tensile strain rate higher than the upper limit of strain rate achievable by the direct tensile test and the Brazilian splitting test. It should be noted that the direct tensile test and the Brazilian splitting test require stress equilibrium in the test specimen, which is not easy to achieve under high-rate loading conditions. However, stress equilibrium is not required to obtain valid data for the spall test, and the spall test can reach the strain rate up to 100 s^{-1}. Therefore, spall test is often used to study the dynamic tensile properties of concrete at high strain rate [3, 11, 12].

Concrete with aggregates is usually assumed to be homogeneous. This assumption might not reflect the actual dynamic mechanical properties of concrete as concrete is made of mortar matrix, aggregates and interfacial transition zones (ITZ) between the aggregates and the mortar matrix [13]. It was found that aggregates in concrete could improve the dynamic mechanical properties of concrete because the strength of aggregate is much higher than that of mortar [3, 9, 12-16]. Therefore, to yield reliable predication on spall test, the effect of aggregates in the concrete specimen should be considered.

Metaconcrete is made by replacing partial or all natural aggregates with engineered aggregates (heavy core coated with soft coating) [4, 17-21]. When stress wave propagates in metaconcrete, the heavy core can absorb the energy applied to metaconcrete through local vibrations, and then attenuate the stress wave in various directions [4, 22]. The region of frequency for which the stress wave is exponentially attenuated is called bandgap. Due to local resonance of heavy core, both the effective mass and effective stiffness of the local resonator made of engineered aggregate could be negative, which is the reason that frequency bandgap could be formed to stop wave propagation in a metaconcrete structure. The more detailed derivation and explanations of achieving effective negative mass and negative stiffness can be found in many previous publications [4, 17, 18, 23-27], which are induced mainly owing to the out-of-phase vibrations of the heavy meta-core with the stress wave.

The study of using the wave-filtering characteristics of metaconcrete to attenuate stress wave generated by impulsive load in metaconcrete structure and mitigate structural damage has been carried out. Jin et al. [17] studied the mechanism of metaconcrete attenuating blast-induced stress wave through analytical derivation and numerical simulation. Mitchell et al. [18-20] numerically demonstrated the effectiveness of metaconcrete in mitigating the effect of blast load on structures. Tan et al. [28] studied the effect of layer numbers of the heavy core against blast and impact loads, and the results revealed that heavy core with more layers can cause wave attenuation in a wider frequency range. Xu et al. [21] investigated the influences of the shape of engineered aggregate and the material properties of components on the bandgap characteristics of engineered aggregate. The response of metaconcrete containing engineered aggregates with various configurations under blast loading was also studied. Jin et al. [4] studied the dynamic tensile properties of metaconcrete through 3D meso-scale simulations, and demonstrated the effectiveness of metaconcrete in mitigating stress wave propagations. However, in the latter study the engineered aggregate was not designed for the desired bandgap for more effective wave propagation mitigations but rather arbitrarily selected. The relationship between the bandgap characteristics of the engineered aggregate and the response of metaconcrete was not investigated in that study. The spall strength of metaconcrete was not studied either.

In this study, engineered aggregate made of heavy core with soft coating is designed via the software COMSOL, to have the targeted bandgap coincide with the primary frequencies of dominant waves propagating in normal concrete (NC) specimen in elastic range to achieve more effective wave propagation mitigations. To demonstrate the effectiveness of using the designed engineered aggregates, a conventional spall test of concrete specimen is studied. A 3D meso-scale model of metaconcrete is built in the software LS-DYNA to simulate the spall test [29]. The metaconcrete is made of mortar, different volume percentages of natural aggregates and engineered aggregates. The natural aggregates and the engineered aggregates are of random size and distribution. The strain rate effect on the strength of mortar and natural aggregate is considered. The influence of particle size of engineered aggregates on the bandgap is investigated. The wave-filtering mechanism of engineered aggregate and the response of the metaconcrete specimen with different bandgap characteristics in spall test are studied. The influence of impulsive load intensity and duration on the response of metaconcrete specimen is also investigated.

2. Numerical simulations of normal concrete specimen

Metaconcrete has sound wave-filtering characteristics, which can only be effective in a specific frequency range (bandgap). When an impulsive load acts on a structure, stress wave induced by the impulsive load propagates in the structure. Therefore, in order to achieve the desired metaconcrete bandgap for effective stress wave mitigation, the frequency distribution of stress wave propagating in specimen NC in the elastic range should be analyzed first via LS-DYNA to identify the primary frequency band.

2.1. Numerical model of normal concrete specimen

In the previous numerical studies, [3, 4, 12, 13, 17, 30, 31], aggregates with various shapes simplified as spherical aggregates yield good predications of concrete under static and high strain rate loads. To simplify the numerical model in this study, the aggregates in concrete mix are simplified to spherical shape with random size and distribution. The grading of aggregate particles determined by the Fuller's curve [32] is also considered in the present study, expressed as,

$$p(d) = 100(\frac{d}{d_{\max}})^n \tag{1}$$

where $p(d)$ is the cumulative percentage of aggregates passing a sieve with aperture diameter d; $d_{\max}$ is the maximum size of aggregate particle; n is the shape parameter of the gradation curve, and varies from 0.45 to 0.7; n is taken as 0.5 in the present study [3].

The specimen NC (Ø74-500 mm) simulated in the present study is based on the NC spall test reported by Wu et al. [11]. The compressive strength of NC is 33.7 MPa [11]. The volume fraction of natural aggregates is 35%, the particle size of natural aggregates is 4-16 mm, and the natural aggregates are divided into three grades (first: 4-8 mm, second: 8-12 mm, and third: 12-16 mm), and the volume percentage of each grade accounts for 14.5%, 11.1% and 9.4% of the total volume, respectively [33, 34]. The ITZ with thickness of 10-50 μm [35-38] is not modelled in the present study. The constant stress solid element with single integration point is used to simulate mortar and natural aggregate. The contact between different components is assumed as perfect bonding, i.e. common nodes to transfer force and displacement. The 3D meso-scale model of specimen NC is shown in Fig. 1. The material parameters of mortar and natural aggregate are given in Table 1.

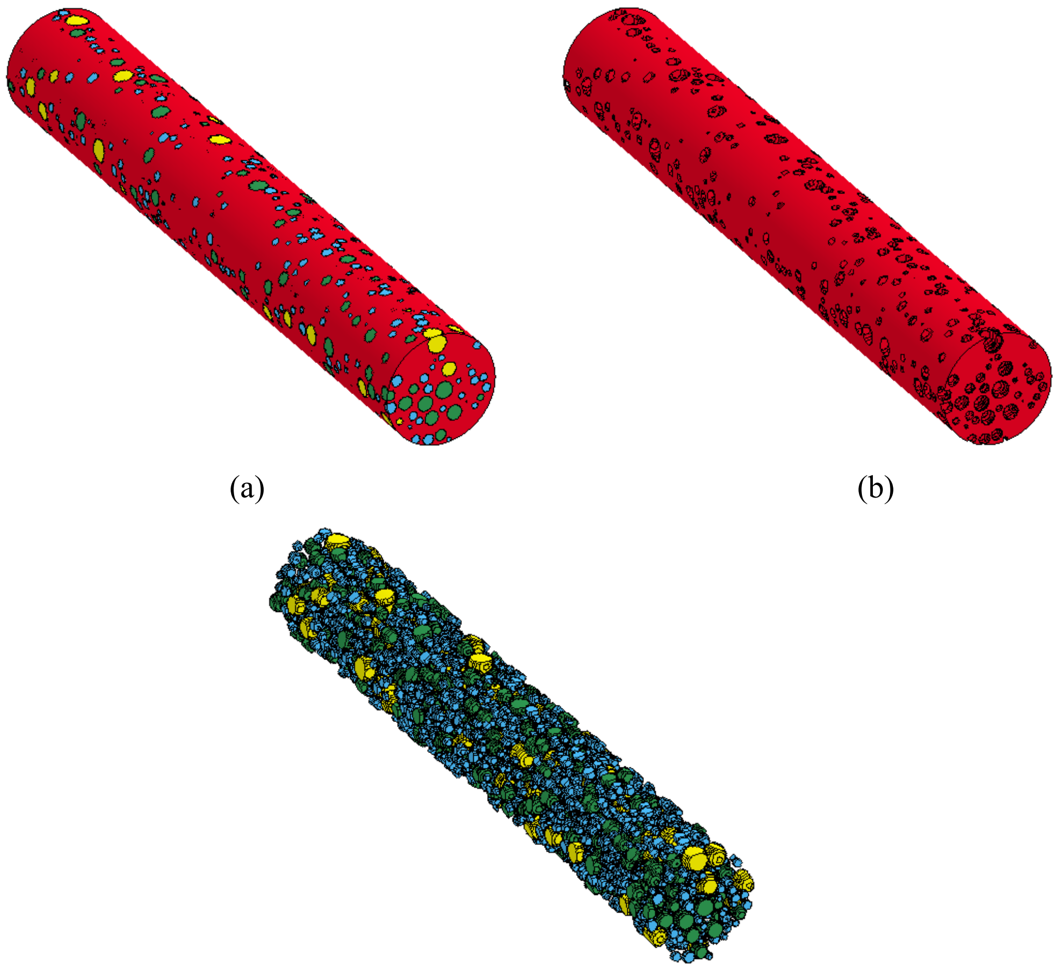

(a) (b)

(c)

Fig. 1 3D meso-scale model of specimen NC

(a) Normal concrete, (b) Mortar matrix, (c) Natural aggregate

Table 1 Material parameters of different components in specimen NC [3, 39]

Material	Density (kg/m^3)	Compressive strength (MPa)	Poisson's ratio
Mortar	2100	34	0.19
Natural aggregate	2600	160	0.16

2.2. Material model and strain rate effect

In the simulation, mortar and natural aggregate are simulated by MAT_CONCRETE_DAMAGE_REL3 (MAT_72R3). This material model is based on the unconfined compressive strength with the consideration of plasticity, shear damage and strain rate effect. In addition to the material parameters given in Table 1, the remaining material parameters can be generated automatically through a built-in algorithm of the material model. Erosion criterion defined by the maximum principal strain of 0.1 is used for mortar and natural aggregate. Both mortar and natural aggregate are strain rate dependent material [39-41]. Therefore, the strain rate effect on the strength of mortar and natural aggregate is considered and described by the dynamic increase factor (DIF).

For compressive strength DIF of mortar [39],

$$\mathrm{CDIF}=0.0419(\log\dot{\varepsilon}_{\mathrm{d}})+1.2165,\quad \dot{\varepsilon}_{\mathrm{d}}<30\mathrm{s}^{-1} \tag{2}$$

$$\mathrm{CDIF}=0.8988(\log\dot{\varepsilon}_{\mathrm{d}})^{2}\text{-}2.8255(\log\dot{\varepsilon}_{\mathrm{d}})+3.4907,\quad 30\mathrm{s}^{-1}\leq\dot{\varepsilon}_{\mathrm{d}}\leq1000\mathrm{s}^{-1} \tag{3}$$

For tensile strength DIF of mortar [41],

$$\mathrm{TDIF}=(\dot{\varepsilon}_{\mathrm{d}}/\dot{\varepsilon}_{\mathrm{ts}})^{\delta},\quad \dot{\varepsilon}_{\mathrm{d}}\leq1\mathrm{s}^{-1} \tag{4}$$

$$\mathrm{TDIF}=\beta(\dot{\varepsilon}_{\mathrm{d}}/\dot{\varepsilon}_{\mathrm{ts}})^{1/3},\quad \dot{\varepsilon}_{\mathrm{d}}>1\mathrm{s}^{-1} \tag{5}$$

where $\delta=1/(1+8f_{\mathrm{cs}}/f_{\mathrm{c0}})$, $\log\beta=6\delta-2$, $f_{\mathrm{c0}}=1\times10^{7}\,\mathrm{Pa}$, $\dot{\varepsilon}_{\mathrm{ts}}=10^{-6}\mathrm{s}^{-1}$ is the quasi-static strain rate, f_{cs} is the quasi-static compressive strength.

For compressive strength DIF of natural aggregate [40],

$$\mathrm{CDIF}=0.0187(\log\dot{\varepsilon}_{\mathrm{d}})+1.2919,\quad 1\mathrm{s}^{-1}\leq\dot{\varepsilon}_{\mathrm{d}}<220\mathrm{s}^{-1} \tag{6}$$

$$\mathrm{CDIF}=1.8547(\log\dot{\varepsilon}_{\mathrm{d}})^{2}\text{-}7.9014(\log\dot{\varepsilon}_{\mathrm{d}})+9.6674,\quad 220\mathrm{s}^{-1}\leq\dot{\varepsilon}_{\mathrm{d}}\leq1000\mathrm{s}^{-1} \tag{7}$$

For tensile strength DIF of natural aggregate [40],

$$\mathrm{TDIF}=0.0598(\log\dot{\varepsilon}_{\mathrm{d}})+1.3588,\quad 10^{-6}\mathrm{s}^{-1}\leq\dot{\varepsilon}_{\mathrm{d}}<0.1\mathrm{s}^{-1} \tag{8}$$

$$\mathrm{TDIF}=0.5605(\log\dot{\varepsilon}_{\mathrm{d}})^{2}+1.381(\log\dot{\varepsilon}_{\mathrm{d}})+2.1256,\quad 0.1\mathrm{s}^{-1}\leq\dot{\varepsilon}_{\mathrm{d}}\leq50\mathrm{s}^{-1} \tag{9}$$

The tensile strength DIF of natural aggregate is assumed as constant when strain rate exceeds 50 s^{-1} [3].

2.3. Calibration of numerical model for normal concrete

Mesh convergence test is conducted by using three mesh sizes of 1 mm, 0.5 mm and 0.1 mm. The impulsive load with 40 MPa amplitude as shown in Fig. 2 is applied [11]. Fig. 3 shows the average stress time histories at the section 150 mm from the incident end of specimen with different mesh sizes. The incident end refers to the position where the impulsive load is applied. As shown, the results obtained from the numerical models with mesh size 0.5 mm and 0.1 mm are almost identical whereas the numerical model with 1 mm mesh size gives different result. Therefore, the mesh size of 0.5 mm is used in the subsequent study. Fig. 4 compares the recorded and numerical simulated strain time histories at the section 150 mm from the incident end of specimen NC. Fig. 5 (a) and (b) compare the failure patterns of specimen NC subjected to the impulsive load as given in Fig. 2. The predicted strain time history and failure pattern agree well with those in the reference [11], which proves the validity of the numerical model.

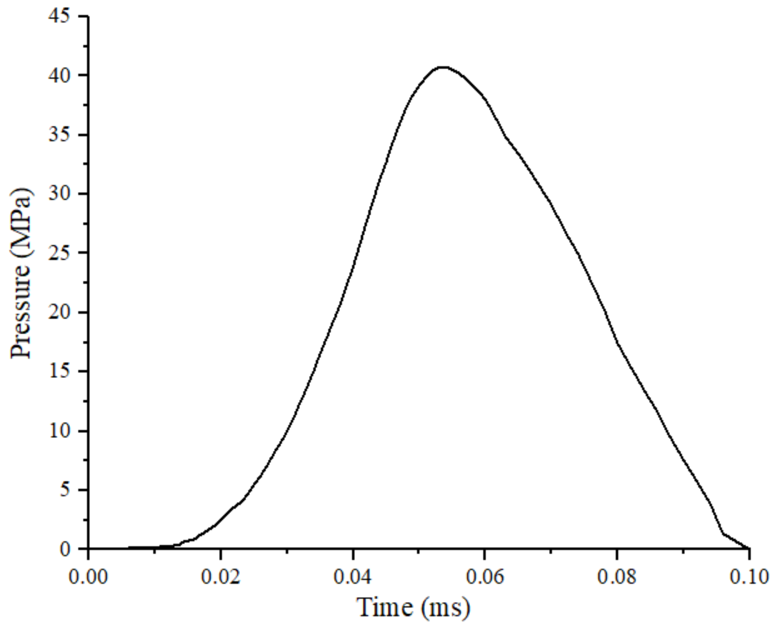

Fig. 2 Impulsive load with 40 MPa amplitude [11]

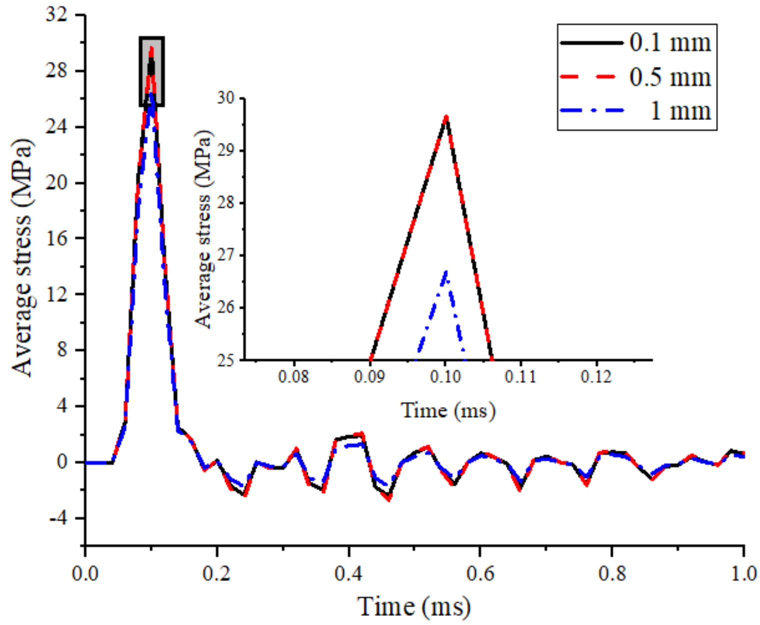

Fig. 3 Average stress at the section 150 mm from the incident end

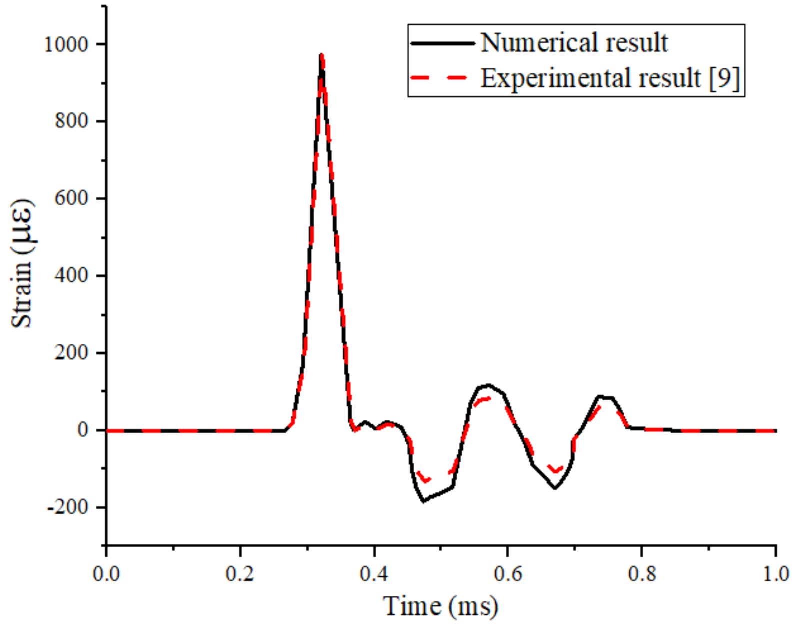

Fig. 4 Strain at the section 150 mm from the incident end

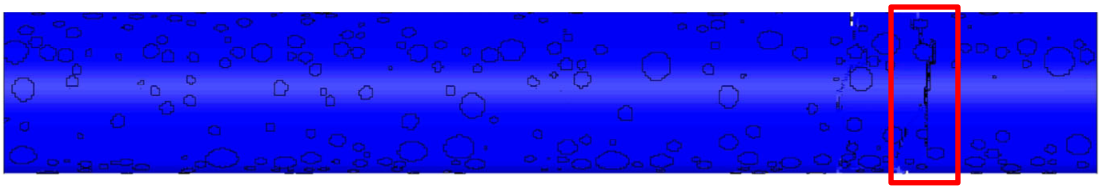

(a)

(b)

Fig. 5 Comparison of failure patterns

(a) Numerical simulation, (b) Experimental result [11]

2.4. Response of normal concrete specimen under impulsive load

To study the response of specimen NC in elastic range, three impulsive loads with lower amplitude (i.e. 8 MPa) and different duration shown in Fig. 6 are applied to specimen NC, respectively [3, 12]. The amplitudes of the applied impulsive loads are less than the yield strength of mortar and natural aggregate used in specimen NC. Therefore, all materials in specimen NC are expected to respond in elastic range before the wave reflection at the end of the specimen. These simulations are carried out to determine the predominant wave frequencies in the specimen for designing the engineered aggregates to have the bandgaps coincide with these predominant wave frequencies. In the present study, four sections CS1-CS4 and a mortar element E1 shown in Fig. 7 are selected to study the stress wave propagation. The sections CS1-CS4 are located at the distance of 5 mm, 250 mm, 495 mm and 400 mm from the loading end, respectively. The element E1 is selected from the rod surface at the section CS4.

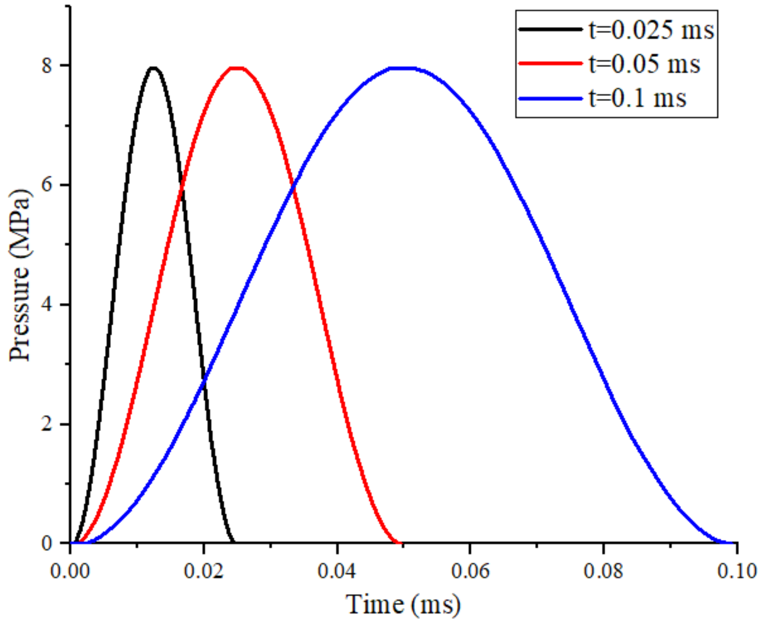

Fig. 6 Impulsive loads with 8 MPa amplitude and different duration [3, 12]

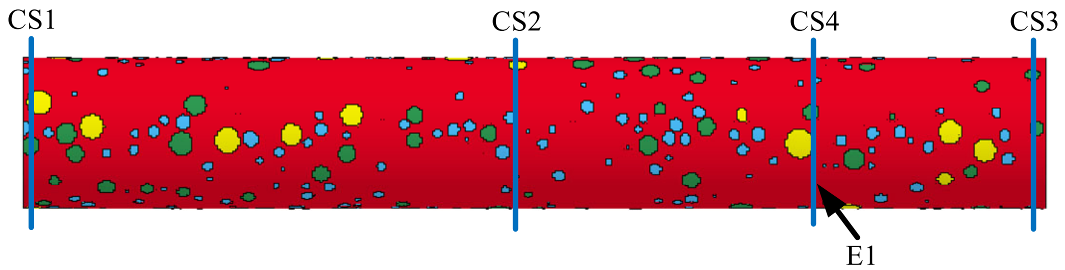

Fig. 7 Schematic diagram of CS1-CS4 and mortar element E1

Without losing generality, the response of specimen NC under impulsive load with 8 MPa amplitude and 0.1 ms duration shown in Fig. 6 is studied first. Fig. 8 shows the time histories of sectional average stress at CS1-CS3. The average stress at the selected section is calculated via dividing the sectional force by the section area. As shown in Fig. 8, when the impulsive load is applied to specimen NC, compressive stress wave generates and propagates in the specimen. The compressive stress wave changes to tensile stress when it is reflected from the free rear surface of the specimen as shown in Fig. 9. The net primary stress at the rear of the specimen is determined by the superposition of the incident stress wave and the reflected stress wave, and is affected by the shape and the duration of the incident stress wave. If the selected section is closer to the free rear end, the net primary stress value is smaller. Therefore, the peak value of the average stress at CS3 shown in Fig. 8 is smaller than that at CS2. When the reflected tensile stress wave reflects again from the loading end, it converts to compressive stress. The superposition of stress wave around the loading end reduces the peak value of the average stress at CS1.

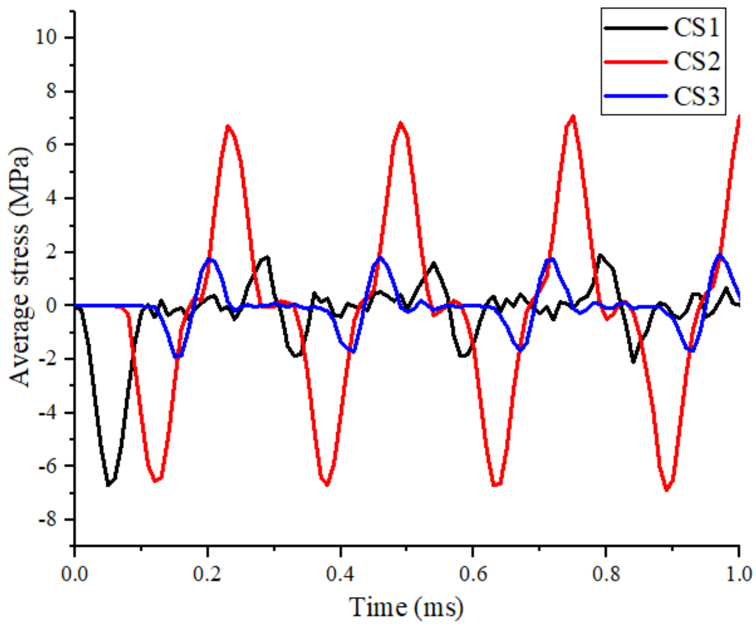

Fig. 8 Average stress time history at CS1-CS3

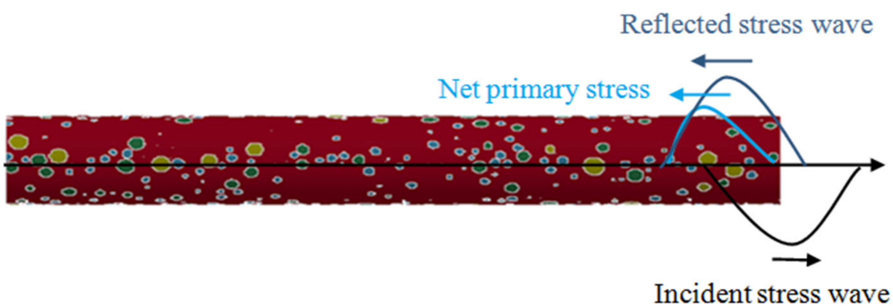

Fig. 9 Reflection of incident stress wave at the rear surface of specimen NC

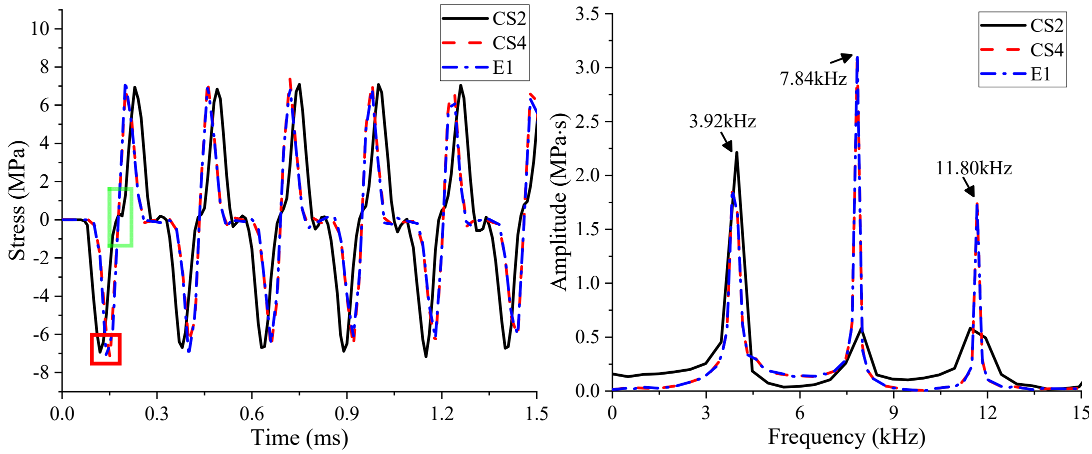

(a) (b)

Fig. 10 Stress time history of the specimen NC

(a) Time domain, (b) Frequency domain

Fig. 10 (a) - (b) show the stress time histories at CS2, CS4 and E1 of specimen NC in the time domain and frequency domain, respectively. As shown in Fig. 10 (a), the first peak of the compressive stress at CS2 appears 0.02 ms earlier than that at CS4 as highlighted in red, which is the time required for stress wave to propagate from CS2 to CS4. The peak values of stress at CS2, CS4 and E1 are similar. The frequency spectra of stress at CS2, CS4 and E1 shown in Fig. 10 (b) are obtained through the Fast Fourier Transform (FFT). The amplitude of stress at CS2, CS4 and E1 peaks at 3.92 kHz, 7.84 kHz and 11.80 kHz as shown in Fig. 10 (b). The amplitudes of wave spectrum at CS4 and E1 are higher than that at CS2 at 7.84 kHz and 11.80 kHz, while the amplitudes at 3.92 kHz at CS4 and E1 are lower than that of CS2, which indicates that high-frequency components of the stress wave become more prominent at CS4, leading to different slopes of stress time history as highlighted in green in Fig. 10 (a). In addition, the spectral peak at 7.84 kHz is higher than that at 3.92 kHz for CS4 and E1. This might be attributed to the boundary reflection effect. In this study, CS4 and E1 are located closer to the end than CS2, the composition of the stress waves becomes more complex near the ends due to the superposition of the incident and reflected stress waves near the ends.

Fig. 11 (a) and (b) show the stress at E1 in specimen NC under three impulsive loads of different duration (i.e. 0.025 ms, 0.05 ms and 0.1 ms) given in Fig. 6 in the time domain and frequency domain, respectively. As shown in Fig. 11 (a), the peak value of stress wave decreases with the reduced impulsive load duration because of the reduced loading impulse imparted into the structure. Under the action of impulsive loads of different duration, the period of stress wave propagating in the specimen is similar since the specimen geometric size and the propagation speed of stress wave in the specimen are the same. The frequency spectrum shown in Fig. 11 (b) is obtained from Fig. 11 (a) by performing Fast Fourier transform (FFT). Fig. 11 (a) shows the stress wave with short period is generated under the impulsive load with shorter duration, which leads to more energy at higher frequencies. This is understandable because the predominant wave frequency is inversely proportional to the wave period. In addition, the geometric dispersion in spall test and the heterogeneity due to the existence of aggregates lead to more stress fluctuations under the impulsive load with shorter duration [3]. As shown in Fig. 11 (b), the amplitudes at 3.92 kHz, 7.84 kHz and 11.80 kHz are higher than those at other frequencies for impulsive loads of different duration, especially when the loading duration is 0.1 ms. When the loading duration is 0.025 ms, more wave energy distributes to higher frequencies, leading to the spectrum peaks at higher frequencies, e.g., the fourth mode at about 16 Hz and the fifth mode at about 23 Hz comparable to those at the first three modes. These results indicate that the stress wave energy concentrates at the wave propagation modes of the specimen, and the energy distributions at different wave modes are dependent on the loading duration or the dominant loading energy distribution over the frequency.

The frequencies of stress waves propagating in a rod can be theoretically predicted by Eq. (10) as

$$f_n = \frac{C_0 n}{2L}, \quad n = 1, 2, 3, \cdots \tag{10}$$

where f_n is the primary wave frequencies, L is the length of specimen, C_0 is the velocity of one-dimensional wave propagation in monolithic material, which can be calculated by $\sqrt{E/\rho}$, in which E and ρ are the elastic modulus and density of the monolithic material. In this study, the propagation velocity of stress wave in the concrete specimen can also be calculated by,

$$C_0 = 2L/\Delta t \tag{11}$$

where Δt is the time difference between two adjacent stress peaks as shown in Fig. 11.

The theoretically calculated first three frequencies of the stress wave propagating in the specimen are given in Table 2. As can be noticed, the theoretically calculated wave frequencies are very close to those obtained in numerical simulations. These results indicate that the primary wave frequencies can be theoretically calculated for designing the desired bandgaps of engineered aggregates. However, the distribution of wave energy at wave propagation modes depends on the loading frequency. The higher is the loading frequency, the more wave energy propagates with higher frequencies. Therefore to determine the target frequency bandgaps for designing the engineered aggregates, proper analysis of wave propagations in structures subjected to the expected load is needed.

Table 2 The theoretically calculated first three wave frequencies in specimen NC

C_0 (m/s)	L (m)	f_1 (kHz)	f_2 (kHz)	f_3 (kHz)
3846.20	0.50	3.85	7.70	11.55

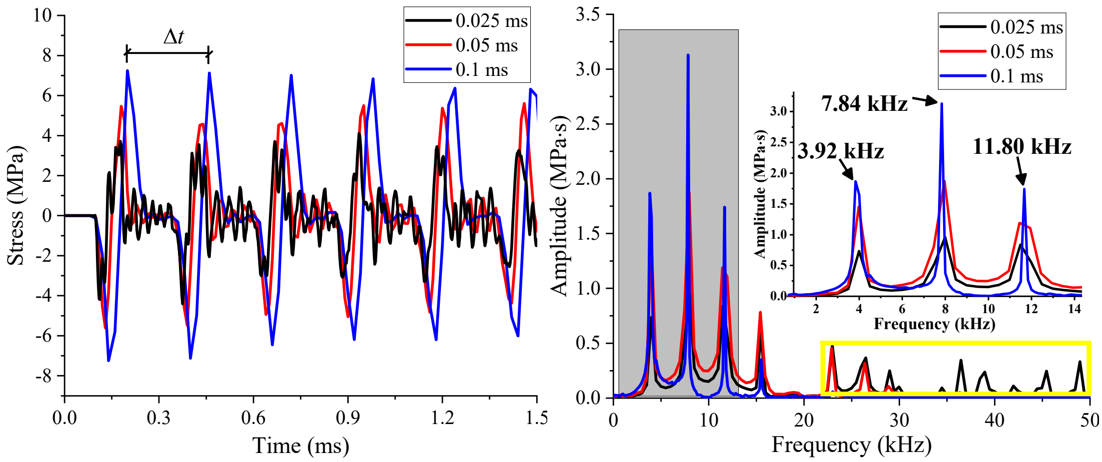

(a) (b)

Fig. 11 Stress time history at E1 of specimen NC under impulsive loads of different duration, (a) Time domain, (b) Frequency domain

3. Design of metaconcrete engineered aggregate

Based on the above results, without loss of generality, in this study three types of engineered aggregates are designed with the central frequency respectively corresponding to the first three wave frequencies at 3.92 kHz, 7.84 kHz and 11.80 kHz to dissipate the energy at these three frequencies. The central frequency of a bandgap is calculated by averaging the upper and lower bound frequencies of an engineered aggregate bandgap. In the present study, the software COMSOL is used to design engineered aggregate with the desired bandgap characteristics. All materials, i.e., soft coating and hard core for the engineered aggregate are assumed as linear elastic, isotropic, continuous, and the material damping is neglected in the numerical model. The size of engineered aggregate designed for metaconcrete in the present study is 12-16 mm, consistent with the third grade of natural aggregates described above in the example specimen considered in this study. The thickness of soft coating is 2 mm, heavy core diameter varies from 8 mm to 12 mm, and the other parameters are unchanged. Fig. 12 shows the schematic diagram of the engineered aggregate designed for metaconcrete in this study.

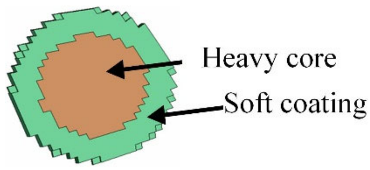

Fig. 12 Schematic diagram of engineered aggregate for metaconcrete

According to the previous studies [4, 21], changing the engineered aggregate size alters its bandgap range even other parameters of the engineered aggregate, e.g. material parameters of heavy core, thickness and material parameters of soft coating are unchanged. In order to achieve the desired central frequency of bandgap for stress wave mitigation, it is necessary to design soft coating with different material parameters via COMSOL. Since the waves in this study propagate only along the axial direction of the specimen, the eigen-frequencies of the engineered aggregate are calculated in the first irreducible Brillouin zone as shown in Fig. 13 [42]. Γ and X are the control point of the first irreducible Brillouin zone, and $\Gamma = 0$, $X = 2\pi/a$, a is the size of engineered aggregate in the numerical model established via COMSOL. The relation between the eigen-frequency and the wave vector is the dispersion relation.

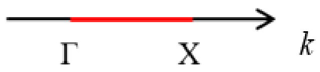

Fig. 13 First irreducible Brillouin zone of metaconcrete unit cell

Table 3 Material parameters of magnetite [43]

Material	Density (kg/m^3)	Elastic modulus (MPa)	Poisson's ratio
Magnetite	5200	6.8×10^4	0.17

Table 4 Bandgap characteristics of engineered aggregates with average diameter 14 mm

Engineered aggregate	EA-A*-3.92	EA-A*-7.84	EA-A*-11.80
Material	Polyurethane	Polyurethane	Polyurethane
Density (kg/m^3)	900	900	900
Elastic modulus (MPa)	7.0	27.8	65.0
Poisson's ratio	0.39	0.41	0.42
Lower bound frequency (kHz)	3.67	7.43	11.13
Upper bound frequency (kHz)	4.17	8.25	12.47
Bandgap width (kHz)	0.50	0.82	1.34

To simplify the design process in this study, engineered aggregate with 14 mm diameter (EA-A*, A* represents average, i.e. 14 mm is the average diameter of all engineered aggregates) is first selected for the design of engineered aggregate. For EA-A*, the average diameter of the heavy core and the thickness of the soft coating are 10 mm and 2 mm, respectively. In this study, magnetite material is selected as the material for heavy core. The material parameters of magnetite are given in Table 3. Polyurethane is selected as the soft coating material [4, 17-20], and the material properties of polyurethane for engineered aggregate with different desired bandgap characteristics are designed in its feasible range via COMSOL [44]. The material parameters of polyurethane coating corresponding to EA-A*-3.92, EA-A*-7.84 and EA-A*-11.80 are given in

Table 4. The bandgap characteristics of these engineered aggregates are also given in Table 4. Fig. 14 (a)-(c) show the dispersion relation of these three types of engineered aggregates corresponding to eigen-frequencies of different orders. As shown in Fig. 14, the bandgaps are found in the region (3.67, 4.17) kHz, (7.43, 8.25) kHz and (11.13, 12.47) kHz, indicating that waves with the frequencies within these regions stop propagating.

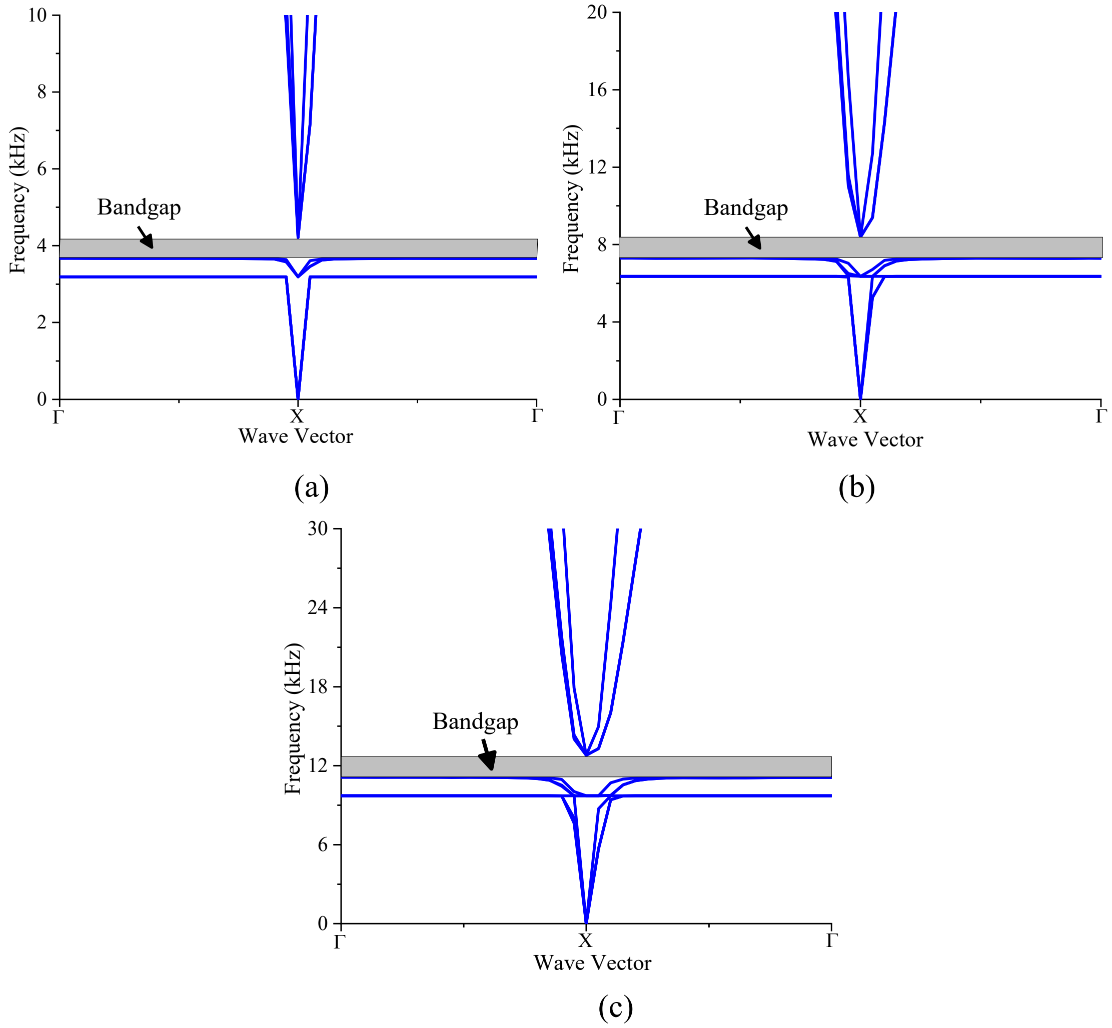

Fig. 14 Dispersion relation of engineered aggregates, (a) EA-A*-3.92, (b) EA-A*-7.84, (c) EA-A*-11.80; Note: wave vector refers to Fig. 13

It should be noted that the diameter of engineered aggregate used to design EA-A* is 14 mm (the average diameter of all the engineered aggregates) with the heavy core diameter 10 mm. It is known that altering the engineered aggregate size changes its frequency bandgap. Keeping the 2 mm thickness of soft coating and the above three polyurethane materials unchanged, varying the heavy core diameter from 8 mm to 12 mm, the bandgaps of these engineered aggregates are calculated via COMSOL. The results indicate that the 12 mm-diameter engineered aggregate with heavy core diameter 8 mm generates the lower bound frequency of bandgap and the 16 mm-diameter engineered aggregate generates the upper bound frequency of bandgap. Combining the bandgaps of these engineered aggregates together, which vary continuously if the heavy core size also varies continuously in the range of 8 mm to 12 mm, the bandgaps of these combined engineered aggregates are calculated and given in Table 5. As can be noticed, both the central frequency and the bandgap width change as compared to those given in

Table 4. The central frequencies do not exactly coincide with the three primary wave frequencies, but are slightly shifted to 3.88 kHz, 7.64 kHz, and 11.79 kHz, however, the width of bandgaps increased. For instance, the bandgap width of Magnetite-11.79 is 2.56 times that of EA-A*-11.80. These bandgaps well cover the primary frequencies of wave propagation.

Table 5 Bandgap characteristics of combined engineered aggregates with magnetite core diameter varying from 8 mm to 12 mm

Engineered aggregate	Magnetite-3.88	Magnetite-7.64	Magnetite-11.79
Diameter range (mm)	12-16	12-16	12-16
Material	Polyurethane	Polyurethane	Polyurethane
Density (kg/m^3)	900	900	900
Elastic modulus (MPa)	7.0	27.8	65.0
Poisson's ratio	0.39	0.41	0.42
Bandgap frequency region (kHz)	3.32-4.44	6.60-8.67	10.07-13.50
Bandgap width (kHz)	1.12	2.07	3.43

4. Numerical simulation of metaconcrete specimen

In order to study the response of metaconcrete in spall test, numerical model of metaconcrete specimen consisting of the designed engineered aggregates is built in LS-DYNA. The geometric size of the metaconcrete specimen is the same as that of specimen NC. By randomly replacing 30% of the third-grade natural aggregate (i.e. 12-16 mm diameter) in specimen NC with engineered aggregates, i.e., the volume percentage of the engineered aggregates is about 2.8% ($P_{eat} = P_a \times P_{ea}$, where P_{eat} is the volume percentage of engineered aggregate in metaconcrete specimen, P_a = 9.4% is the volume percentage of the third-grade natural aggregate in NC and P_{ea} =30% is the volume percentage of engineered aggregates used to replace the third-grade natural aggregate) of the total specimen volume, the numerical model of metaconcrete specimen is established. The size and distribution of aggregates in metaconcrete specimen are the same as those in specimen NC. The constant stress solid element with single integration point is used to simulate magnetite core and polyurethane coating. The contact between polyurethane coating and mortar matrix is assumed as perfectly bonded. The magnetite core and polyurethane coating are modelled as linear elastic.

5. Response of metaconcrete specimen in spall test under impulsive load

5.1. Response of metaconcrete composed of only one kind of engineered aggregate

In order to analyze the attenuation effect of designed engineered aggregate on the stress wave generated by impulsive load in metaconcrete, the response of metaconcrete specimen (M-11.79) composed of only one kind of engineered aggregates (Magnetite-11.79) is also studied. The impulsive load with 8 MPa amplitude and 0.1 ms duration shown in Fig. 6 is applied to specimen M-11.79. Two elements shown in Fig. 15, E2 (mortar matrix element) and E3 (magnetite core element), at the section CS4 shown in Fig. 7 are selected to study the response of specimen M-11.79.

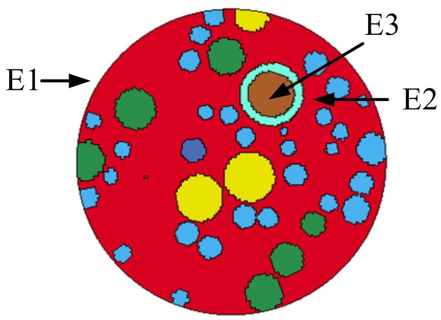

Fig. 15 Schematic diagram of E1-E3

Fig. 16 (a) shows the displacement time histories of E2 and E3 of specimen M-11.79. For comparison, the displacements of these elements in specimen NC are also illustrated in Fig. 16 (b). As shown, relative movement between the magnetite core and the mortar matrix is observed in specimen M-11.79 because of the low deformation resistance of the polyurethane coating, and no relative movement occurs in specimen NC. Fig. 17 shows the time histories of kinetic energy and internal energy absorbed by different components in specimen M-11.79. As shown, the energy absorbed by the mortar matrix and the natural aggregate varies between 1.02 J and 1.14 J and the input energy is partially absorbed by the designed engineered aggregates owing to local vibrations of the magnetite cores.

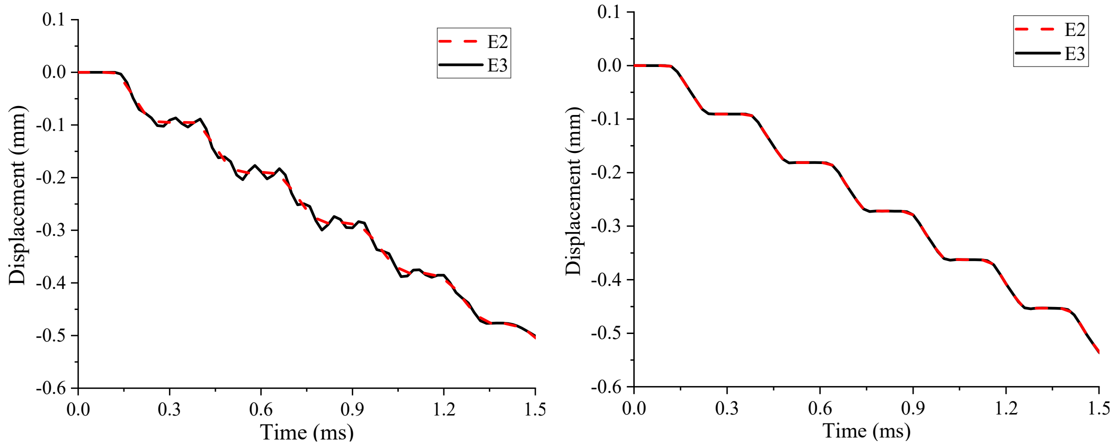

(a) (b)

Fig. 16 Displacement time histories of E2 and E3

(a) Specimen M-11.79, (b) Specimen NC

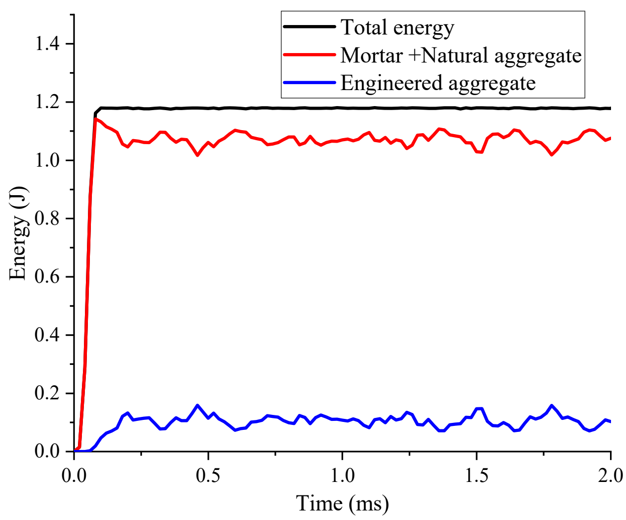

Fig. 17 Time history of energy absorption of specimen M-11.79

Fig. 18 (a) and (b) show the stress time histories at E1 of specimen M-11.79 and specimen NC in the time domain and frequency domain, respectively. As compared to specimen NC, the second tensile stress peak at E1 is delayed by 3×10^{-2} ms. It is because the existence of Magnetite-11.79 engineered aggregate in specimen M-11.79 reduces the propagation velocity of stress wave. The first compressive stress peak at E1 in specimen M-11.79 is reduced by 17.3% as compared to that of specimen NC (as highlighted in green at t = 0.15 ms). The compressive stress wave induced by the impulsive load changes to a tensile stress wave when it is reflected from the rear surface of the specimen. As shown in Fig. 18 (a), the first tensile stress peak at E1 in specimen M-11.79 is reduced by 21.6% as compared to that of specimen NC (as highlighted in orange at t = 0.21 ms). The attenuation percentage of the first tensile stress peak is higher than that of the first compressive stress peak in specimen M-11.79 because the stress wave propagated through more numbers of engineered aggregates. When the first compressive stress peak and the first tensile stress peak appear at E1 of specimen M-11.79, the energy absorbed by engineered aggregates is 0.08 J and 0.13 J, respectively. Fig. 18 (b) shows the stress at E1 in specimen M-11.79 and specimen NC in the frequency domain. The amplitude corresponding to 11.79 kHz in the response of specimen M-11.79 is effectively reduced. In addition, due to the reduced propagation velocity of stress wave in metaconcrete, the period of stress wave propagating in specimen M-11.79 slightly increases as shown in Fig. 18 (a). Therefore, more energy in specimen M-11.79 shifts to the lower frequency, as shown in Fig. 18 (b).

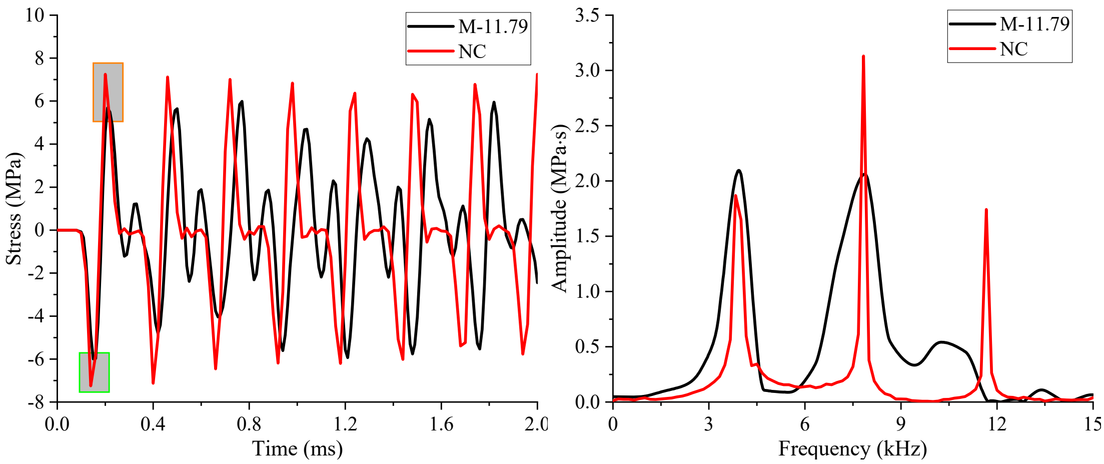

(a) (b)

Fig. 18 Stress time histories at E1 in specimen M-11.79 and specimen NC

(a) Time domain, (b) Frequency domain

5.2. Response of metaconcrete composed of combined engineered aggregates

As shown in Fig. 11 (b), the response of specimen NC shows relatively high amplitude at 3.92 kHz, 7.84 kHz and 11.80 kHz in frequency domain. To mitigate stress wave propagations, the combined engineered aggregates (Magnetite-3.88, Magnetite-7.64 and Magnetite-11.79) as described above are used to compose metaconcrete to investigate the effect of using engineered aggregates with multiple bandgaps on the metaconcrete dispersion relation and the stress wave attenuation. The same impulsive load with 8 MPa amplitude and 0.1 ms duration shown in Fig. 6 is applied to specimen MG.

Fig. 19 shows the energy absorption time histories of different components in specimen MG. Due to local resonance of the magnetite core as shown in Fig. 16 (a), part of the stress wave energy converts to kinetic energy of the cores of the engineered aggregates, therefore the energy absorbed by engineered aggregates increases gradually with the propagation of stress wave inside specimen MG with the vibrations of more number of cores being activated. It is also found that the energy absorbed by the engineered aggregates significantly increases and the energy absorbed by the mortar and natural aggregates decreases as compared with specimen M-11.79 as shown in Fig. 17.

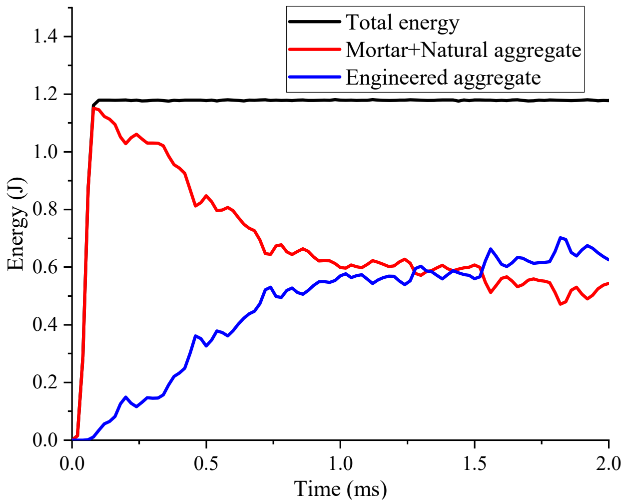

Fig. 19 Energy absorption time history of specimen MG

Fig. 20 (a) and (b) show the stress at E1 in specimen M-11.79, specimen MG and specimen NC in the time domain and frequency domain, respectively. As shown in Fig. 20 (a), the first compressive stress peak at E1 of specimen MG is reduced by 15.6% as compared to that of specimen NC as highlighted in green. The first tensile stress peak at E1 of specimen MG is reduced by 29.8% as compared to that of specimen NC, which is higher than that (21.6%) of specimen M-11.79 (as highlighted in orange). With the increase of the reflection number of stress wave within specimen MG, the energy absorbed by the engineered aggregates increases, and the peak values of compressive stress and tensile stress at E1 of specimen MG attenuate more significantly than those of specimen M-11.79. As shown in Fig. 20 (b), the amplitudes of stress wave in specimen MG are reduced at 3.88 kHz, 7.64 kHz and 11.79 kHz, which fall in the bandgaps given in Table 5. Therefore, stress wave can be further attenuated by using engineered aggregates with multiple bandgaps as compared to that when only one type of engineered aggregate is used.

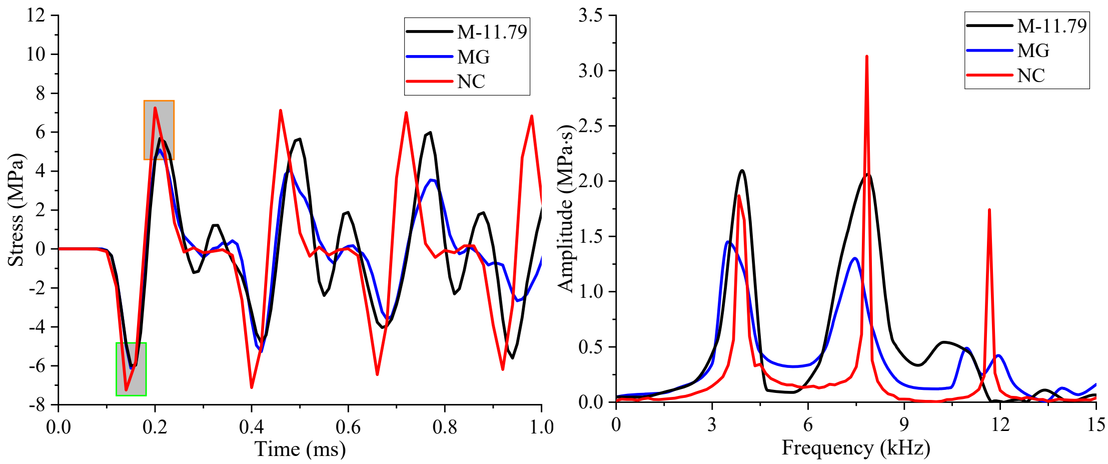

(a) (b)

Fig. 20 Stress at E1 of three structures (M-11.79, MG, NC)

(a) Time domain, (b) Frequency domain

5.3. Effect of impulsive load duration on the response of metaconcrete

In order to study the influence of impulsive load duration or frequency contents on the response of metaconcrete in spall test, impulsive loads with three duration (i.e., 0.025 ms, 0.05ms and 0.1 ms) shown in Fig. 6 are applied to specimen MG. Fig. 21 (a) - (c) show the comparison of stress time histories at E1 for specimen NC and specimen MG under impulsive loads of three different duration, respectively. As shown in Fig. 21, the first compressive stress wave peaks of specimen MG corresponding to the impulsive loads with duration 0.025 ms, 0.05 ms and 0.1 ms are reduced by 0.2%, 15% and 15.6% as compared to that of specimen NC, respectively (as highlighted in green).

The corresponding first tensile stress wave peaks of specimen MG are reduced by 0.19%, 24.7% and 29.8% as compared to that of specimen NC, respectively (as highlighted in blue). These results indicate the engineered aggregates are ineffective in mitigating the first stress wave peaks when loading duration is 0.025 ms. This is because the three bandgaps of the designed engineered aggregates for specimen MG only cover the first three wave propagation frequencies. As discussed above and shown in Fig. 11 (b), the responses of specimen NC have more peaks at higher frequencies outside these three bandgaps under the impulsive loads with the duration of 0.025 ms. Therefore, the engineered aggregates in specimen MG are ineffective in mitigating the wave energies corresponding to these high frequency modes. However, the metaconcrete with engineered aggregates is still effective in mitigating stress wave propagations at frequencies fall in the three bandgaps. As shown in Fig. 21 (a), with the propagation of stress wave in the specimen, the wave amplitudes are reduced substantially as compared to those in NC.

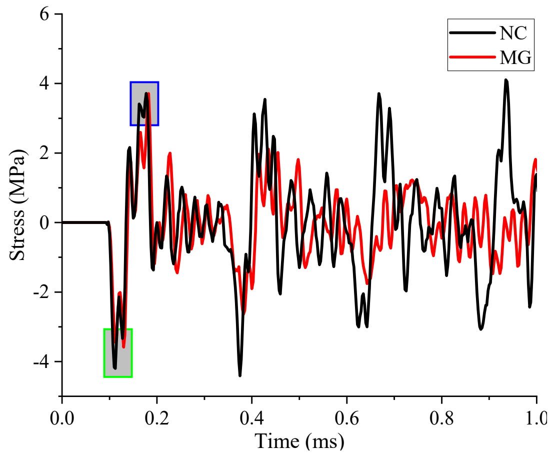

(a)

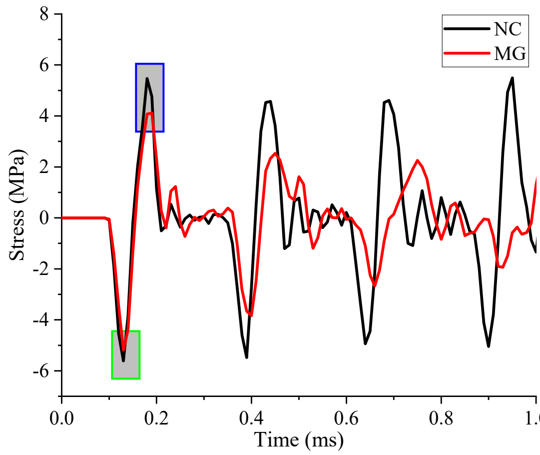

(b)

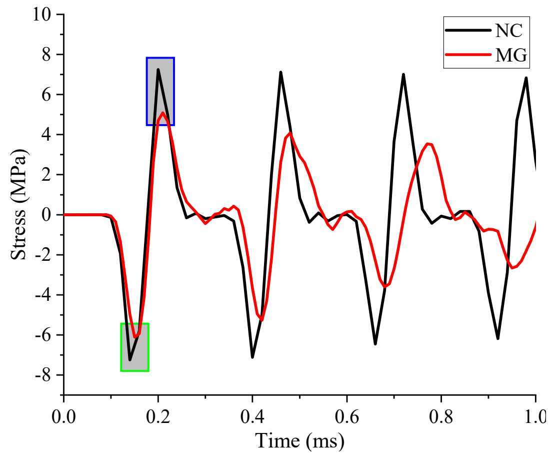

(c)

Fig. 21 Stress time histories at E1 in specimen MG and specimen NC corresponding to impulsive loading with different duration, (a) 0.025 ms, (b) 0.05ms, (c) 0.1 ms

5.4. Response of metaconcrete under high amplitude impulsive load

The engineered aggregates used to compose metaconcrete in this study are designed based on the frequency band of stress wave in specimen NC in elastic range and in the above simulations the concrete material damage is not considered. To study the coupled influences of nonlinear inelastic response and material damage with the local vibrations of engineered aggregates on wave propagation, the impulsive loads with 20 MPa and 60 MPa amplitudes, and 0.1 ms duration shown in Fig. 22 are applied to specimen MG and specimen NC, respectively. It should be noted that nonlinear response and damage of concrete material absorb wave energy, therefore attenuate stress wave amplitude; however, on the other hand, they also change the predominant frequency of stress wave propagating in the concrete specimen, making the predominant wave frequency outside the bandgaps of the designed metaconcrete, hence resulting in the metaconcrete less effective in attenuating stress wave propagation. This section studies these combined effect, namely the plastic deformation of concrete material and engineered aggregates on wave propagation mitigations.

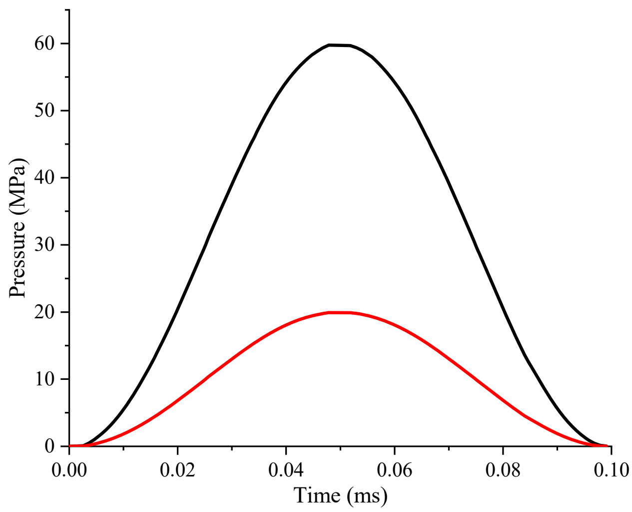

Fig. 22 Impulsive loads with 20 MPa and 60 MPa amplitudes and 0.1 ms duration

Fig. 23 (a) and (b) show the spall damage patterns of specimen NC and specimen MG under the impulsive load with 20 MPa amplitude, respectively. As shown in Fig.

23, these two specimens experience tensile fracture damage at different locations under the same impulsive load, the damage of specimen MG is more serious than that of specimen NC. Based on the previous studies [3, 12], the spall strength can be predicted based on

$$\sigma = \frac{\rho C_0 \Delta V_{\mathrm{pb}}}{2} \tag{12}$$

where ρ is the material density, ΔV_{pb} is the pullback velocity recorded at the rear surface of specimen.

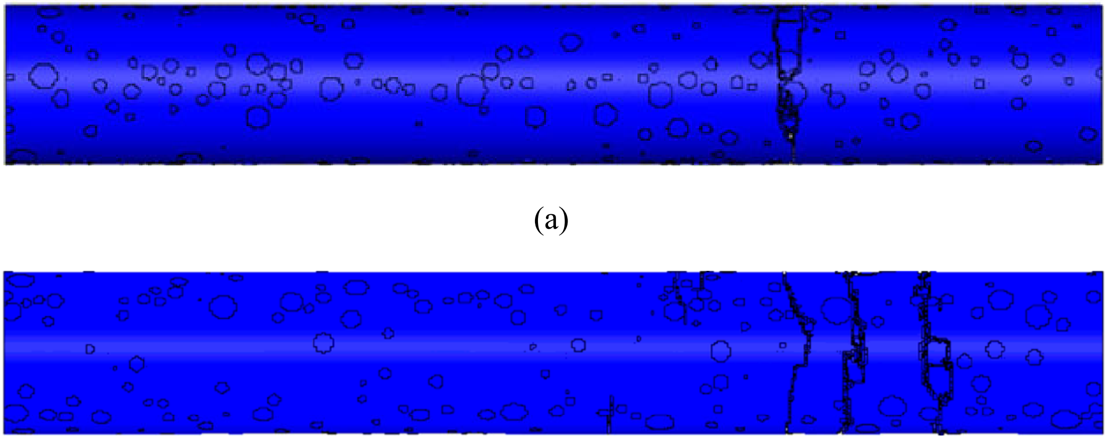

(a)

(b)

Fig. 23 Comparison of spall damage patterns of different specimens under impulsive load of 20 MPa, (a) Specimen NC, (b) Specimen MG

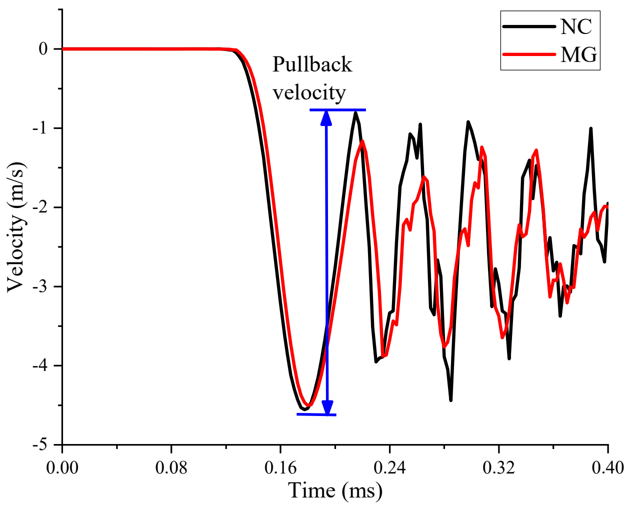

Fig. 24 Pullback velocity of specimen NC and specimen MG

Fig. 24 shows the pullback velocity time histories of specimen NC and specimen MG under the action of impulsive load with 20 MPa amplitude. Table 6 gives the parameters used for calculating the spall strength of NC and MG. According to Eq. 12, the spall strength of MG is reduced by 22.3% as compared to that of NC. Fig. 25 shows the maximum principal strain contours of specimen NC and specimen MG before the specimens experience spall damage under the impulsive load with 20 MPa amplitude. Specimen NC experiences spall damage owing to the net primary stress caused by the superposition of the reflected tensile stress and the incident compressive stress. For specimen MG, polyurethane coating is softer than that of magnetite core and mortar matrix. Since soft coating is prone to deform while the surrounding mortar is brittle, the soft coating makes the mortar vulnerable to be damaged, which reduces the concrete strength. Local damage of mortar matrix around the engineered aggregates leads to tensile fracture of the metaconcrete specimen. In other words, existing of soft coating in metaconcrete reduces the concrete strength, and hence the spall strength.

Table 6 Parameters used for calculating the spall strength of specimen materials

Material	Density (kg/m^3)	Wave velocity (m/s)	Pullback velocity (m/s)	Spall strength (MPa)
NC	2237.80	3846.20	3.70	15.92
MG	2234.80	3571.43	3.10	12.37

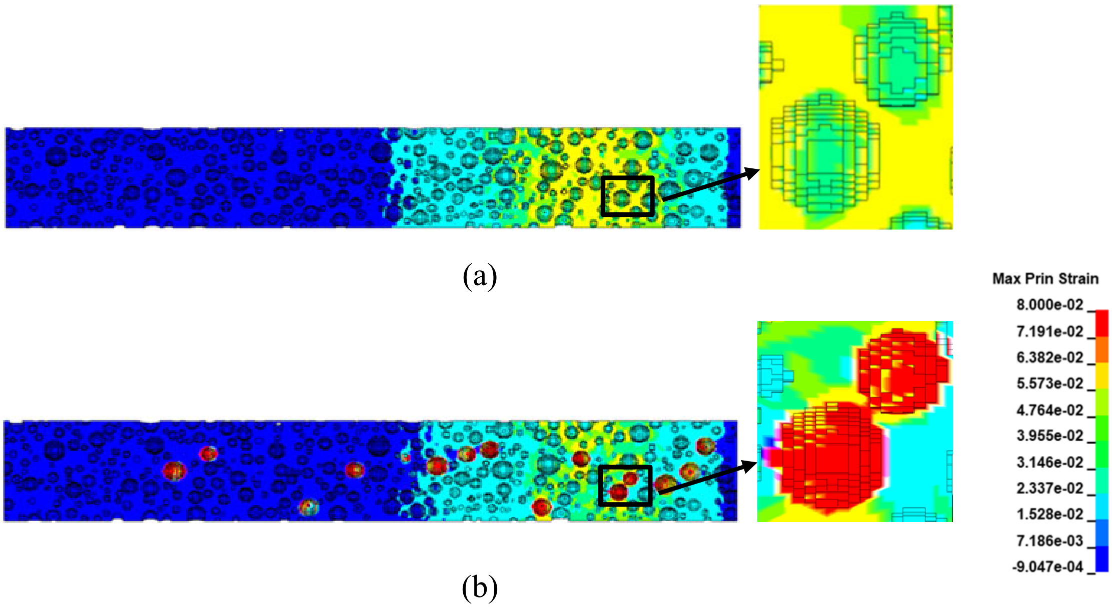

Fig. 25 Maximum principal strain contours of mortar matrix of different specimens

under impulsive load of 20 MPa at t = 0.2 ms, (a) Specimen NC, (b) Specimen MG

The above observations indicate that although metaconcrete can reduce stress wave propagation owing to the local vibrations of engineered aggregates that attract and consume certain amount of wave energy, it also reduces the strength of concrete because of the soft coating of the engineered aggregates. To further demonstrate that the soft coating reduces the concrete strength and its effect on impulsive loading resistance, another impulsive loading with amplitude of 60 MPa is applied to the two specimens. Fig. 26 shows the damage patterns of specimen NC and specimen MG at t = 1 ms under the 60 MPa impulsive load. As shown, localized compressive damage as highlighted in red is found at specimen MG because of the existence of polyurethane coating with lower stiffness, but no compressive damage occurs at specimen NC because of the strain rate effect which makes the dynamic compressive strength of concrete higher than 60 MPa. The compressive damage of metaconcrete could dissipate a substantial amount of input energy [17] and reduce wave propagation. Due to the resultant effect of localized damage and the wave mitigation mechanism of metaconcrete, the spall damage of specimen MG is less severe than that of specimen NC, which indicates superior performance of metaconcrete if it is used in a sacrificial protective structure against high impact load. Nonetheless, the problem of reducing the concrete strength by the soft coating of engineered aggregate needs be considered if metaconcrete is used in a normal structure.

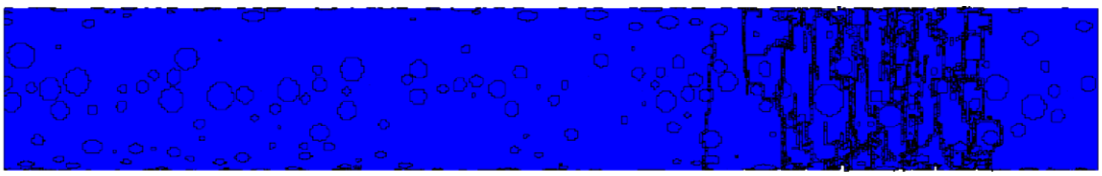

(a)

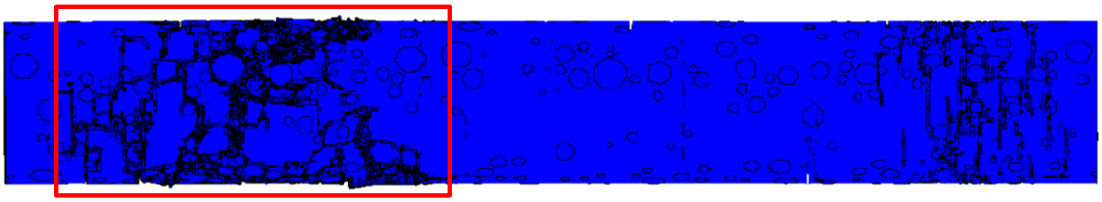

(b)

Fig. 26 Comparison of damage patterns of different specimens under impulsive load of 60 MPa, (a) Specimen NC, (b) Specimen MG

6. Conclusion

This study investigates the stress wave propagation and spall behavior of metaconcrete with randomly distributed aggregates by using 3D meso-scale modelling. A 3D meso-scale model of metaconcrete with randomly distributed aggregates is simulated in the software LS-DYNA. The strain rate effect on the strength of mortar and natural aggregate is considered in the numerical simulation. The engineered aggregates with different bandgap characteristics are designed via the software COMSOL. The effects of single or multiple engineered aggregate bandgaps, the duration and intensity of impulsive load on the dynamic response of metaconcrete in spall test are studied. The main conclusions are given below.

1. The response of normal concrete (NC) in elastic stage can be used to identify the primary wave frequencies for the design of engineered aggregate to achieve the desired bandgap, which can more effectively attenuate the expected stress wave propagation in the metaconcrete specimen.

2. Because stress wave energy concentrates at multiple frequencies, using engineered aggregates with multiple bandgaps is more effective in mitigating wave propagation. The first tensile peak of the selected element of specimen MG considered in this study can be reduced by 29.8% as compared to that of specimen NC.

3. Although local vibrations of engineered aggregates mitigate stress wave propagation, its soft coating reduces the concrete strength and the spall strength. Therefore, metaconcrete can be used to construct sacrificial structures. The problem of concrete strength reduction by the soft coating of engineered aggregate needs be considered if metaconcrete is used for normal structures.

7. Acknowledgement

The authors are grateful for the financial support from the Australian Research Council (ARC) via Laureate Fellowship FL180100196.

Reference

[1] M.R. Sharma, A.K. Singh, G.S. Benipal, Elastic Stability of Concrete Beam-Columns, International

Journal of Structural Stability and Dynamics, 17 (2017).
[2] K.A. Gomathi, A. Rajagopal, Dynamic performance of reinforced concrete slabs under impact and blast loading using a plasticity based approach, International Journal of Structural Stability and Dynamics, 20 (2020).
[3] G. Chen, Y.F. Hao, H. Hao, 3D meso-scale modelling of concrete material in spall tests, Materials and Structures, 48 (2015) 1887-1899.
[4] H.X. Jin, W.S. Chen, H. Hao, Y.F. Hao, Numerical study on impact resistance of metaconcrete (in Chinese), Science China (Physics, Mechanics & Astronomy), 49 (2019).
[5] J. Li, H. Hao, Numerical study of concrete spall damage to blast loads, International Journal of Impact Engineering, 68 (2014) 41-55.
[6] A. Brara, F. Camborde, J.R. Klepaczko, C. Mariotti, Experimental and numerical study of concrete at high strain rates in tension, Mechanics of Materials, 33 (2001) 33-45.
[7] H. Schuler, C. Mayrhofer, K. Thoma, Spall experiments for the measurement of the tensile strength and fracture energy of concrete at high strain rates, International Journal of Impact Engineering, 32 (2006) 1635-1650.
[8] Tedesco J.W, Ross C.A, M. P.B, Numerical analysis of high strain rate concrete direct tension tests, Computers & Structures, 40 (1991) 313-327.
[9] D.M. Yan, L. Gao, Dynamic properties of concrete in direct tension, Cement and Concrete Research, 36 (2006) 1371-1378.
[10] J.T. Gomez, A. Shukla, A. Sharma, Static and dynamic behavior of concrete and granite in tension with damage, Theoretical and Applied Fracture Mechanics, 36 (2001) 37-49.
[11] H.J. Wu, Q.M. Zhang, F.L. Huang, Q.K. Jin, Experimental and numerical investigation on the dynamic tensile strength of concrete, International Journal of Impact Engineering, 32 (2005) 605-617.
[12] P.B. Xu, H. Xu, H.M. Wen, 3D meso-mechanical modeling of concrete spall tests, International Journal of Impact Engineering, 97 (2016) 46-56.
[13] X.Q. Zhou, H. Hao, Mesoscale Modelling Of Concrete Tensile Failure Mechanism At High Strain Rates, Computers & Structures, 86 (2008) 2013-2026.
[14] Y. Hao, H. Hao, X.H. Zhang, Numerical analysis of concrete material properties at high strain rate under direct tension, International journal of impact engineering, 39 (2012) 51-62.
[15] X.D. Chen, S.X. Wu, J.K. Zhou, Experimental and modeling study of dynamic mechanical properties of cement paste, mortar and concrete, Construction and Building Materials, 47 (2013) 419-430.
[16] K. Wu, B. Chen, W. Yao, D. Zhang, Effect of coarse aggregate type on mechanical properties of high-performance concrete, Cement and Concrete Research, 31 (2001) 1421-1425.
[17] Y. Shi, J. Wang, J. Cui, Experimental studies on fragments of reinforced concrete slabs under close-in explosions, International Journal of Impact Engineering, (2020) 103630.
[18] S.J. Mitchell, A. Pandolfi, M. Ortiz, Metaconcrete: designed aggregates to enhance dynamic performance, Journal of the Mechanics and Physics of Solids, 65 (2014) 69-81.
[19] S.J. Mitchell, A. Pandolfi, M. Ortiz, Investigation of elastic wave transmission in a metaconcrete slab, Mechanics of Materials, 91 (2015) 295-303.
[20] S.J. Mitchell, A. Pandolfi, M. Ortiz, Effect of brittle fracture in a metaconcrete slab under shock loading, Journal of Engineering Mechanics, 142 (2016) 04016010.
[21] C. Xu, W.S. Chen, H. Hao, The influence of design parameters of engineered aggregate in metaconcrete on bandgap region, Journal of the Mechanics and Physics of Solids, 103929 (2020).

[22] E.J.P.M. Jr, E.D. Nobrega, S.F. Rodrigues, C.A. Jr, J.M.C.D. Santos, Wave attenuation in elastic metamaterial thick plates: Analytical, numerical and experimental investigations, International Journal of Solids and Structures, 204-205 (2020) 138-152.

[23] H. Huang, C. Sun, G. Huang, On the negative effective mass density in acoustic metamaterials, International Journal of Engineering Science, 47 (2009) 610-617.

[24] Z.Y. Liu, C.T. Chan, P. Sheng, Three-component elastic wave band-gap material, Physical Review B, 65 (2002) 165116.

[25] Z.Y. Liu, C.T. Chan, P. Sheng, Analytic model of phononic crystals with local resonances, Physical Review B, 71 (2005) 014103.

[26] Z.Y. Liu, X.X. Zhang, Y.W. Mao, Y. Zhu, Z.Y. Yang, C.T. Chan, P. Sheng, Locally resonant sonic materials, science, 289 (2000) 1734-1736.

[27] W. Zhou, Muhammad, W. Chen, Z. Chen, C. Lim, Actively controllable flexural wave band gaps in beam-type acoustic metamaterials with shunted piezoelectric patches, European Journal of Mechanics - A/Solids, 77 (2019) 103807.

[28] K.T. Tan, H. Huang, C. Sun, Blast-wave impact mitigation using negative effective mass density concept of elastic metamaterials, International Journal of Impact Engineering, 64 (2014) 20-29.

[29] L. Jin, M.J. Liu, R.B. Zhang, X.L. Du, 3D meso-scale modelling of the interface behavior between ribbed steel bar and concrete, Engineering Fracture Mechanics, 239 (2020) 107291.

[30] Z. Li, H. Chen, The development trend of advanced building materials, in: Proceeding of the first international forum on advances in structural engineering, 2006.

[31] C. Jin, N. Buratti, M. Stacchini, M. Savoia, G. Cusatis, Lattice discrete particle modeling of fiber reinforced concrete: Experiments and simulations, European Journal of Mechanics - A/Solids, 57 (2016) 85-107.

[32] P. Wriggers, S.O. Moftah, Mesoscale models for concrete: Homogenisation and damage behaviour, Finite Elements in Analysis and Design, 42 (2006) 623-636.

[33] Y.W. Chen, J.L. Feng, H. Li, Z.F. Meng, Effect of coarse aggregate volume fraction on mode II fracture toughness of concrete, Engineering Fracture Mechanics, 242 (2020).

[34] L. Jin, W.X. Yu, X.L. Du, W.X. Yang, Meso-scale simulations of size effect on concrete dynamic splitting tensile strength: Influence of aggregate content and maximum aggregate size, Engineering Fracture Mechanics, 230 (2020) 106979.

[35] W.A. Tasong, C.J. Lynsdale, J.C. Cripps, Aggregate-cement paste interface - Part I. Influence of aggregate geochemistry, Cement & Concrete Research, 29 (1999).

[36] E.K.K. Nambiar, K. Ramamurthy, Air‐void characterisation of foam concrete, Cement & Concrete Research, 37 (2007) 221-230.

[37] J.Z. Xiao, W.G. Li, D.J. Corr, S.P. Shah, Effects of interfacial transition zones on the stress–strain behavior of modeled recycled aggregate concrete, Cement and Concrete Research, 52 (2013) 82-99.

[38] E.A. Rodrigues, O.L. Manzoli, L.A.G. Bitencourt Jr., T.N. Bittencourt, 2D mesoscale model for concrete based on the use of interface element with a high aspect ratio, International Journal of Solids and Structures, 94-95 (2016) 112-124.

[39] Y.F. Hao, H. Hao, Numerical evaluation of the influence of aggregates on concrete compressive strength at high strain rate, International Journal of Protective Structures, 2 (2011) 177-206.

[40] Y.F. Hao, H. Hao, Numerical Investigation of the dynamic compressive behaviour of rock materials at high strain rate, Rock Mechanics and Rock Engineering, 46 (2013) 373-388.

[41] L. Malvar, J. Crawford, Dynamic increase factors for concrete. In: Twenty-eighth DDESB seminar,

Orlando, Florida, (1998).
[42] Z. Cheng, Z. Shi, Novel composite periodic structures with attenuation zones, Engineering Structures, 56 (2013) 1271-1282.
[43] C. DeArmitt, Magnetite, In: Palsule S. (eds) Polymers and Polymeric Composites: A Reference Series. Springer, Berlin, Heidelberg, (2016).
[44] W. Zhang, B. Xue, Elastic modulus adjustable polyurethane composition, scaffold composite and preparation method thereof, in, China, 2017.